Huang et al. Nanoscale Research Letters (2017) 12:491
DOI 10.1186/s11671-017-2260-0

Nanoscale Research Letters

NANO EXPRESS Open Access

Fabrication of Ordered Nanopattern by using ABC Triblock Copolymer with Salt in Toluene

Hailiang Huang, Benbin Zhong, Xihong Zu*, Hongsheng Luo, Wenjing Lin, Minghai Zhang, Yazhou Zhong and Guobin Yi*

Abstract

Ordered nanopatterns of triblock copolymer polystyrene-*block*-poly(2-vinylpyridine)-*block*- poly (ethylene oxide) (PS-*b*-P2VP-*b*-PEO) have been achieved by the addition of lithium chloride (LiCl). The morphological and structural evolution of PS-*b*-P2VP-*b*-PEO/LiCl thin films were systematically investigated by varying different experimental parameters, including the treatment for polymer solution after the addition of LiCl, the time scale of ultrasonic treatment and the molar ratio of Li^+ ions to the total number of oxygen atoms (O) in PEO block and the nitrogen atoms (N) in P2VP block. When toluene was used as the solvent for LiCl, ordered nanopattern with cylinders or nanostripes could be obtained after spin-coating. The mechanism of nanopattern transformation was related to the loading of LiCl in different microdomains.

Keywords: Ultrasound, Microphase separation, Triblock copolymer, Lithium chloride

Background

Recently, ion/block copolymers (BCPs) hybrids have become highly attractive materials due to their flexibility, process stability, self-assembling ability and novel features of inorganic components such as electronic, magnetic and optical properties [1–3]. Spatz and co-workers created fused silica substrates with nanopillars on both sides with 99.8% transmittance and 0.02% reflectance, which was helpful for many laser applications [4]. Black et al. fabricated densely packed silicon nanotextures with feature sizes smaller than 50 nm by block copolymer self-assembly to enhance the broadband antireflection of solar cells [5]. Morris et al. fabricated Si nanowire array by self-assembly of block copolymer with LiCl, which showed the possible application in the area of photonics and photoluminescence [6].

Compared with diblock copolymers (diBCPs), ABC triblock copolymer (triBCPs) can assemble into new morphologies such as periodic arrays of core/shell spheres and cylinders, tetragonal lattices of cylinders, and bicontinuous and tricontinuous ordered mesophases [7–15]. However, ion/triBCPs hybrids are rarely reported [16]. To further explore the novel properties of ABC triBCPs and develop more performance requirements, it is necessary to study the ion/triBCPs hybrids.

The addition of salts into the BCPs is one of effective way to obtain ordered nanopatterns. Researchers have found that polyethylene oxide (PEO) [17–19], polymethyl methacrylate (PMMA) [20], poly(ε-caprolactone) (PCL) [21] or polyvinyl pyridine (PVP) [22, 23] are ion-dissolving blocks, and polystyrene (PS) [24] is a non-conducting block. Wang and co-workers suggested that the selection of metal ions to blocks was primarily due to the large solvation energy when the lithium salts associate with the polar PEO domains, leading to a large increase in the effective segregation strength with lithium salt loading [25, 26].

In previous experiments [6, 17, 27], the co-solvents for salts are frequently used because of the solubility of salts and the efficiency of coordination between salts and BCPs. Russell et al. continuously stirred after the mixture of LiCl in tetrahydrofuran (THF) and polystyrene-*block*-poly(methyl methacrylate) (PS-*b*-PMMA) toluene solution with moderate heating until most of THF was

* Correspondence: zxhong329@126.com; ygb702@163.com
School of Chemical Engineering and Light Industry, Guangdong University of Technology, Guangzhou, Guangdong 510006, People's Republic of China

Springer Open

© The Author(s). 2017 **Open Access** This article is distributed under the terms of the Creative Commons Attribution 4.0 International License (http://creativecommons.org/licenses/by/4.0/), which permits unrestricted use, distribution, and reproduction in any medium, provided you give appropriate credit to the original author(s) and the source, provide a link to the Creative Commons license, and indicate if changes were made.

evaporated and the solutions became clear. And they spent a great deal of time (about 24 h) on stir and post-treatment (solvent vapor annealing and thermal annealing) to obtain ordered microphase-separated nanostructure [17, 28].

Herein, we demonstrated a simple and convenient approach to generate various ordered nanopatterns of ion/triBCPs hybrids by spin-coating method without any further treatments. Morphological and structural variations of PS-*b*-P2VP-*b*-PEO thin films with different salt concentrations were examined by adjusting various processing parameters. This work indicated that the coordination between PS-*b*-P2VP-*b*-PEO and LiCl-toluene could be accelerated by ultrasonic treatment for fabricating ordered nanopattern.

Methods

Materials

Triblock copolymer polystyrene-*block*-poly(2-vinylpyridine)-*block*-poly(ethylene oxide)(PS- *b*-P2VP-*b*-PEO, 45,000 g/mol, 16,000 g/mol, 8500 g/mol, M_w/M_n = 1.05) was purchased from Polymer Source Inc. and used without further purification in this study. Anhydrous lithium chloride (LiCl, 95%+, AR) was purchased from Tianjin Fuchen Chemical Reagents Factory. Toluene (99 + %), ethanol and N,N-Dimethylform amide (DMF, analytical grade) were purchased from Tianjin Damao Chemical Co. Ltd. Silicon(Si) wafer was purchased from No.46 Research Institute of China Electronics Technology Group Corporation (CETC).

Sample Preparation

Si wafers were cleaned in DMF, ethanol and deionized water under ultrasonic for 30 min at room temperature, respectively. 0.1 wt% PS-*b*-P2VP-*b*-PEO toluene solution was stirred for 24 h at room temperature. And LiCl was dispersed in toluene by ultrasound for 30 min at room temperature. Then various volume of LiCl toluene solution was immediately added to the PS-*b*-P2VP-*b*-PEO micellar solutions. Those mixtures were treated by different ways to trigger complexation between Li^+ ions and polymer chains. The resultant solutions were spin-coated immediately onto the substrate at 3000 rpm for 1 min after filtration. At last, the films were dried under nitrogen at room temperature to remove the residual solvent.

Characterization

Atomic force microscope (AFM) in SCANASYST-AIR mode (Nanoscope-V Multimode 8, Bruker Inc., Germany) by using a silicon cantilever (spring constant 5 N/m and resonant frequency ~ 150 kHz, Budget Sensors, Bulgaria Ltd.) was used to investigate the morphological features of PS-*b*-P2VP-*b*-PEO thin films. High-resolution transmission electron microscopy (HRTEM) measurement was carried out on a JEM-2100HR (JEOL, Japan) operated at 200 kV accelerating voltage. Film samples for TEM were prepared onto carbon-coated copper grids. Those samples were exposed to I_2 vapor for certain time period. Fourier transform infrared (FT-IR) spectra were recorded with a Nicolet 6700 (Thermo, USA) spectrophotometer in the range of 4000–400 cm^{-1} with KBr plates. Ultraviolet–visible (UV-vis) spectra were obtained on a UV-2450(Shimadzu, Japan) spectrophotometer. X-ray photoelectron spectroscopy (XPS) measurements were performed on ESCALAB 250 (Thermo, USA) with Al Ka excitation.

Results and Discussion

Morphology of Pure PS-*b*-P2VP-*b*-PEO Thin Film

When 0.1 wt% PS-b-P2VP-b-PEO toluene solution was stirred for 24 h and spin-coated on silicon wafer, nanoporous patterns could be observed in Fig. 1. The average size of nanopores was about 22 nm.

Dispersion of LiCl in Toluene

Dispersions of LiCl in toluene with various aging times are shown in Fig. 2. Toluene was not a good solvent for LiCl. So suspension with unstable status could be seen after ultrasonic treatment (Fig. 2a). It was noticeable that little sedimentation phenomenon was observed when the aging time was 5 min (Fig. 2d). Therefore, the prepared suspension should be used immediately after ultrasonic treatment.

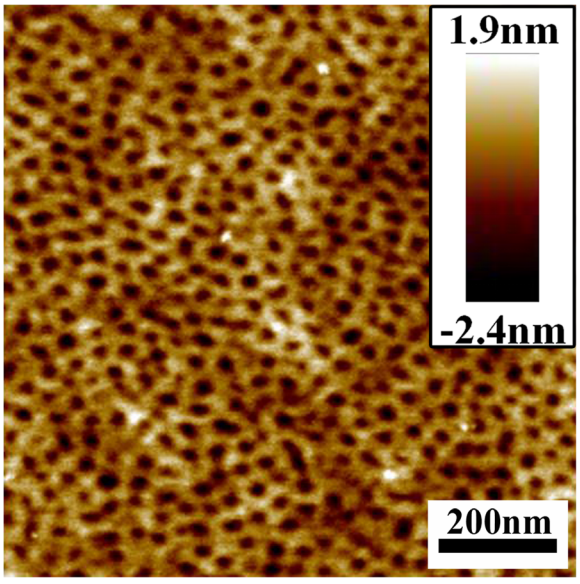

Fig. 1 AFM height images of PS-*b*-P2VP-*b*-PEO films spin-coated from 0.1 wt% PS-*b*-P2VP-*b*-PEO toluene solution

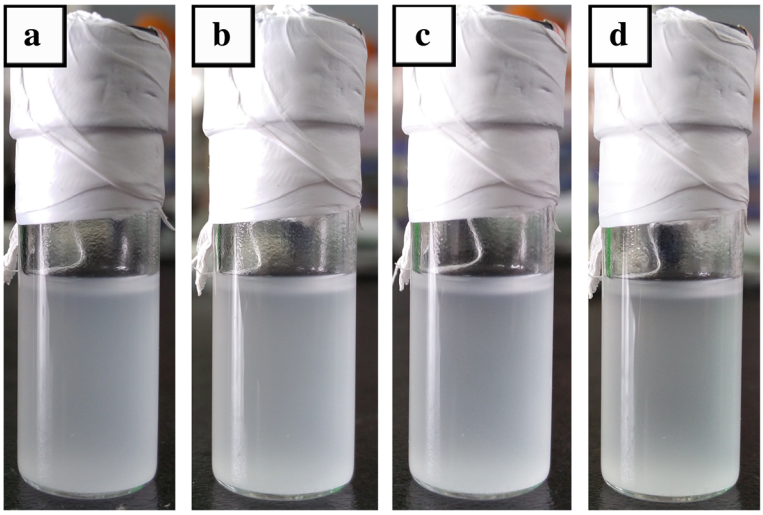

Fig. 2 Dispersion of LiCl in toluene after ultrasonic treatment without and with different aging time: (**a**) without aging time, (**b**) 1 min, (**c**) 3 min, (**d**) 5 min

Effect of Methods to Trigger the Coordination between LiCl and Polymer Chains

Generally, stir and post-treatment are required for polymer solution containing metal salts in order to trigger the coordination between salts and polymer chains for fabrication of ordered nanostructure, which takes a lot of time [22, 28]. And the ultrasound is the simple way to accelerate the coordination between metal ions and block copolymer [29–31]. In order to demonstrate the advantage of ultrasonic treatment in this work, different methods were used after the mix of LiCl-toluene and triblock copolymer solution when the molar ratio of Li^+ ions to the total number of oxygen atoms (O) in PEO block and the nitrogen atoms (N) was 1:32.2([Li^+]:[O + N] = 1:32.2). When the mixed solution was stirred (1500 rpm) for 30 min at room temperature and then spin-coated onto substrate, no distinct ordered structure was observed in Fig. 3a. When the mixed solution was stirred at 1500 rpm for 30 min at 75 °C and then spin-coated onto substrate, disordered cylindrical microdomains appeared in Fig. 3b. When the mixed solution was placed in ultrasonic cleaner for 30 min at room temperature, microphase-separated nanopattern with cylindrical microdomain was obtained obviously in Fig. 3c after spin-coating. The energy provided by sound waves was able to disrupt the larger aggregates of the micelles. And the sound waves could further increase the diffusion rate of metal ions in the solution, so the loading of Li^+ ions in micelles were expected to happen much faster than the conventional stirring method. This result indicated that ultrasonic treatment was a useful method to improve the efficiency of coordination between Li^+ ions and polymer chains.

Effect of Time Scale

In order to investigate the time scale of ultrasonic treatment, the mixed solution ([Li^+]:[O + N] = 1:32.2) was

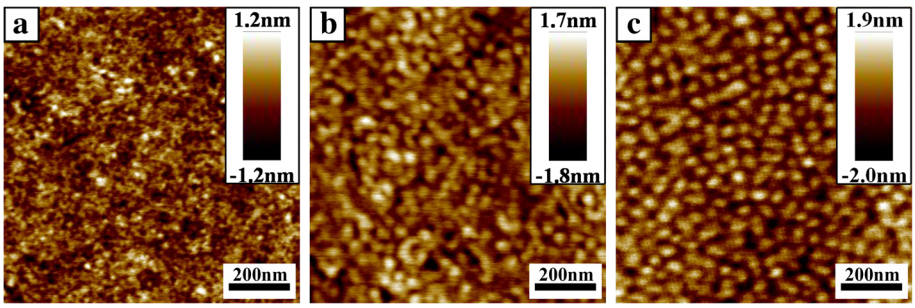

Fig. 3 AFM height images of PS-*b*-P2VP-*b*-PEO films spin-coated from 0.1 wt% toluene solution with different methods after the addition of LiCl-toluene when the molar ratio of Li^+ ions to the total number of oxygen atoms (O) in PEO block and the nitrogen atoms (N) is 1:32.2: (**a**) 1500 rpm stirring for 30 min at room temperature, (**b**) 1500 rpm stirring for 30 min at 75 °C, (**c**) ultrasonic treatment for 30 min at room temperature

placed in ultrasonic cleaners for various times before spin-coating. When the time was 7.5 min (Fig. 4a), the nanoporous morphology was similar to the film in Fig. 1. Compared with the film in Fig. 1, the number and the average size of nanopores decreased, which indicated that Li^+ ions began to load in PS-*b*-P2VP-*b*-PEO polymer chains after 7.5 min. The Li^+ ions loaded in polymer chains would increase with the time increasing. Parts of nanopores were connected when the time increased to 15 min (Fig. 4b). When the time was 22.5 min, the nanopattern exhibited a coexistence of nanostripes and cylinders (Fig. 4c). When the time was prolonged to 30 min, microphase-separation with cylindrical microdomains occurred obviously (Fig. 3c). As the time extended to 37.5 min, the coexistence of nanostripes and cylindrical microdomains appeared again (Fig. 4d). From above results, when the time was less than 30 min, the complexation between Li^+ ions and PS-*b*-P2VP-*b*-PEO was accelerated by ultrasonic treatment so that more and more Li^+ ions were coordinated with PS-*b*-P2VP-*b*-PEO, resulting in transition of nanopattern from nanoporous array to cylindrical array. When the time was more than 30 min, the energy provided by sound waves would break the coordination of Li^+ ions and polymer chains so that disordered nanopattern was found instead of the cylindrical array. Therefore, the time of ultrasonic treatment should be controlled in appropriate range to obtain obvious microphase-separated nanopattern.

Effect of LiCl Content in PS-b-P2VP-b-PEO Thin Films

The addition of LiCl has significant effects on morphology since Li^+ ions could be loaded in P2VP and PEO blocks [17–19, 22, 23]. And the molar ratio ([Li^+]:[O + N]) was varied in our work (Fig. 5).

When the molar ratio was 1:40.25, the nanopattern of stripes was obtained (Fig. 5a). When the molar ratio decreased to 1:32.2, nanopattern with cylindrical microdomains could be seen in Fig. 3c. As the molar ratio was 1:24.15, a lot of nanopores were connected to show the tendency from nanopores pattern transform to nanostripes (Fig. 5b). When the molar ratio was 1:16.1, disordered nanopores become the overall morphology (Fig. 5c). The average size of holes was larger than the film in Fig. 1. As the molar ratio further decreased to 1:8.05, a few of nanopaores was observed in Fig. 5d. The average diameter of these pores was more than 40 nm. From above results, an order-to-disorder transition was shown in Fig. 5 by

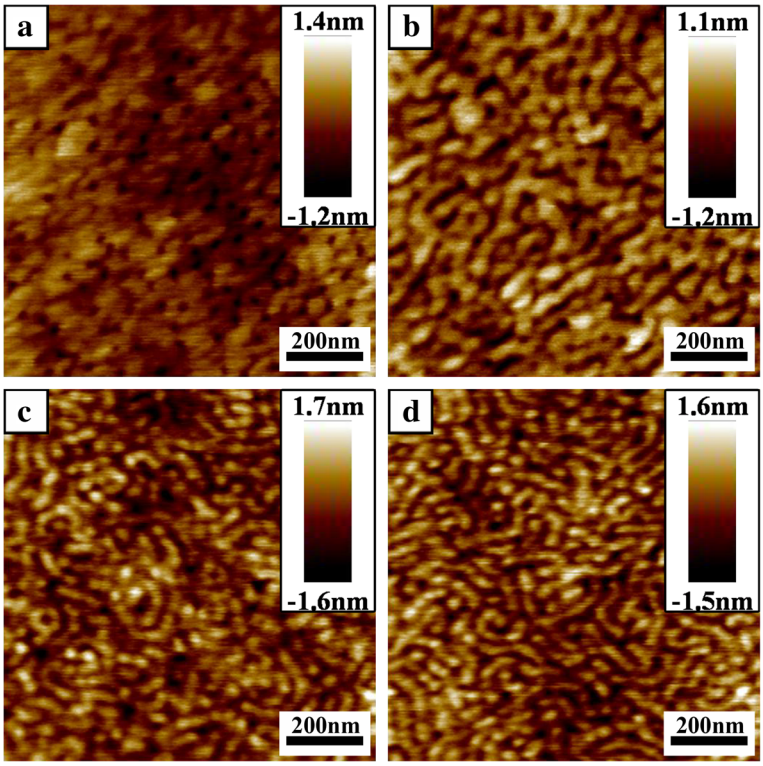

Fig. 4 AFM height images of PS-*b*-P2VP-*b*-PEO films spin-coated from 0.1 wt% polymer-LiCl toluene solution with various time scale of ultrasonic treatment when the molar ratio of Li^+ ions to the total number of oxygen atoms (O) in PEO block and the nitrogen atoms (N) is 1:32.2: (**a**) 7.5 min, (**b**) 15 min, (**c**) 22.5 min, (**d**) 37.5 min

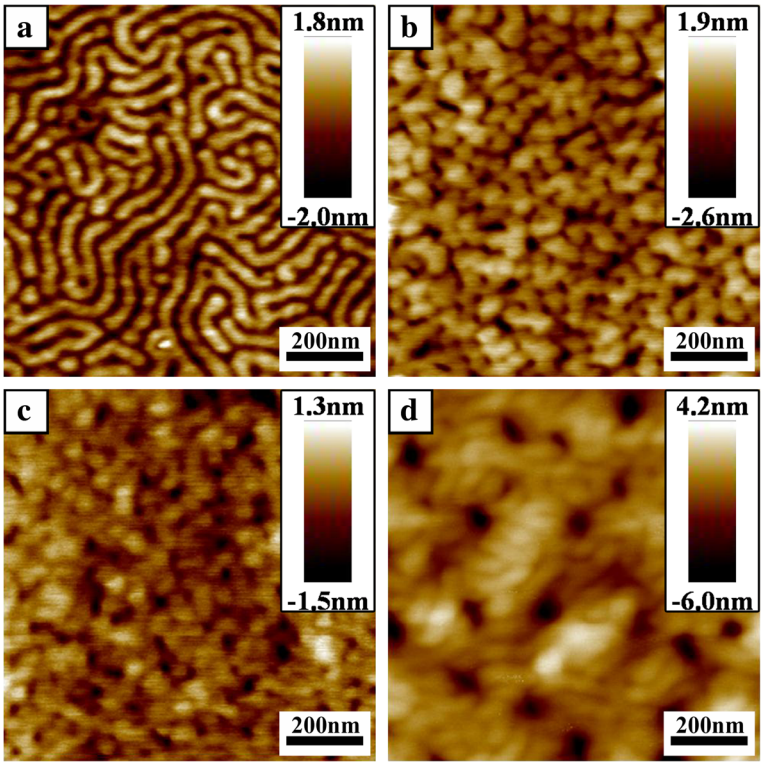

Fig. 5 AFM height images of PS-*b*-P2VP-*b*-PEO films spin-coated from 0.1wt%polymer-LiCl toluene solution with various molar ratio of Li^+ ions to ethylene oxide moieties and pyridine groups: (**a**) 1:40.25, (**b**) 1:24.15, (**c**) 1:16.1, (**d**) 1:8.05

controlling the addition of LiCl in ion/polymer hybrids. The change of LiCl loaded in polymer chains was the reason for the morphological transition. The LiCl loading in polymer chains increased with decreasing molar ratio ([Li^+]:[O + N]), leading to the different phase behaviors of the PS-*b*-P2VP-*b*-PEO/LiCl hybrids. And the ordered arrangements of PS-*b*-P2VP-*b*-PEO/LiCl hybrids were formed with the critical amount of LiCl loaded.

Microdomains Location of Three Blocks in PS-*b*-P2VP-*b*-PEO Thin Films

In order to explore the microdomain location of the three blocks in PS-*b*-P2VP-*b*-PEO thin film under different conditions, those samples were exposed to I_2 vapor for certain period before TEM measurement.

The PS-*b*-P2VP-*b*-PEO thin film without LiCl exhibited an array of dark rings after the selective staining of P2VP blocks, indicating that the periphery of the hole

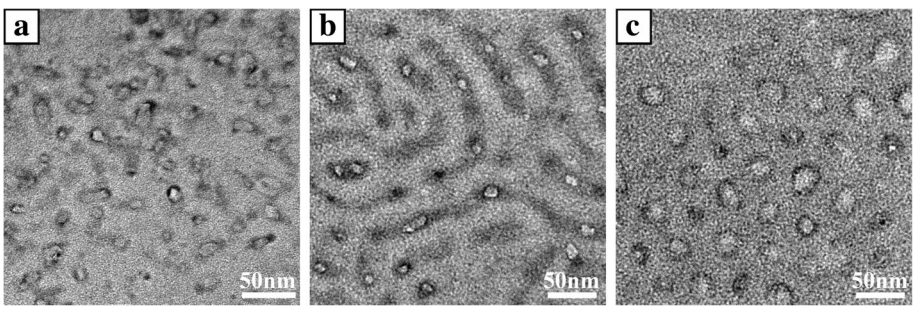

Fig. 6 TEM images of PS-*b*-P2VP-*b*-PEO film after I_2 staining with and without LiCl: (**a**) without LiCl, (**b**) with LiCl-toluene and the molar ratio of LiCl to ethylene oxide moieties and pyridine groups was 1:40.25, (**c**) with LiCl-toluene and the molar ratio of LiCl to ethylene oxide moieties and pyridine groups was 1:32.2

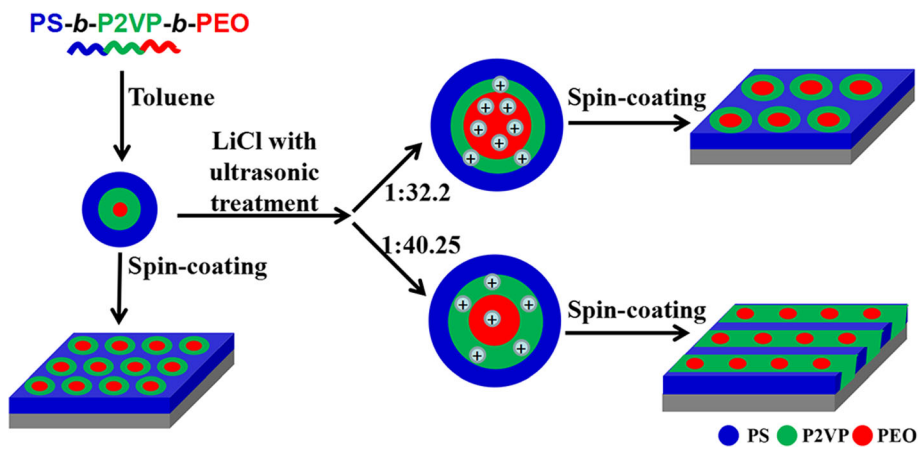

Fig. 7 Schematic illustration of the fabrication of PS-*b*-P2VP-*b*-PEO nanopattern with and without Li^+ ions

corresponded to P2VP blocks (Fig. 6a). Thus, the rest of the hole should match with PEO blocks. The continuous matrix was PS blocks. The average outer diameter of the dark rings was about 21 nm and the average inner diameter of the dark rings was about 16 nm.

When the molar ratio ([Li^+]:[O + N]) was 1:40.25 after I_2 selective staining, the nanopattern of stripes was obtained (Fig. 6b). The bright regions of the spheres were depressed in striated structure. The bright regions were PEO blocks and the rest of stripes were P2VP microdomains. Hence, the continuous matrix was PS blocks. Distinct dark particulates (of LiOH presumably) were observed in P2VP domains [32]. The average diameter of PEO domains was about 17 nm, which was similar to the average domain size of PEO blocks in Fig. 6a. And the P2VP domains transformed from dark rings to stripes. This result indicated that most of Li^+ ions were preferentially coordinated with P2VP blocks when the molar ratio was 1:40.25.

When the molar ratio ([Li^+]:[O + N]) decreased to 1:32.2, an array of dark rings could also be seen (Fig. 6c) after I_2 selective staining. The dark rings were P2VP microdomains and the bright regions were PEO blocks. The continuous matrix was PS blocks. The average outer diameter of dark rings was about 32 nm, and the average inner diameter of dark ring was about 26 nm. It was demonstrated that the cylindrical domains in Fig. 3c were core-shell structure. The outer shell was P2VP blocks and the core was PEO blocks. Compared with the film in Fig. 6a, the PEO microdomains were obviously swelled and the P2VP domains slightly increased. Compared with the film in Fig. 6b, this result indicated that more Li^+ ions were coordinated with PEO blocks with more LiCl in PS-b-P2VP-b-PEO thin film.

The difference of Fig. 6b, c can be explained as shown in Fig. 7. Because of the selectivity of toluene for three blocks, the nanostructure of PS-*b*-P2VP-*b*-PEO micelles in toluene was core-shell structure. Considering the sequence of the three blocks in PS-*b*-P2VP-*b*-PEO, PS blocks were the outer shell. The inner shell was P2VP domain and the core was PEO blocks. When the molar ratio ([Li^+]:[O + N]) was 1:40.25, the Li^+ ions were mainly focused on the inner shell of P2VP blocks because of the limited content of LiCl and the resistance of P2VP inner shell. As a result, only a few of Li^+ ions were coordinated with PEO microdomains. When the molar ratio ([Li^+]:[O + N]) was 1:32.2, the interaction parameter of Li^+ ions

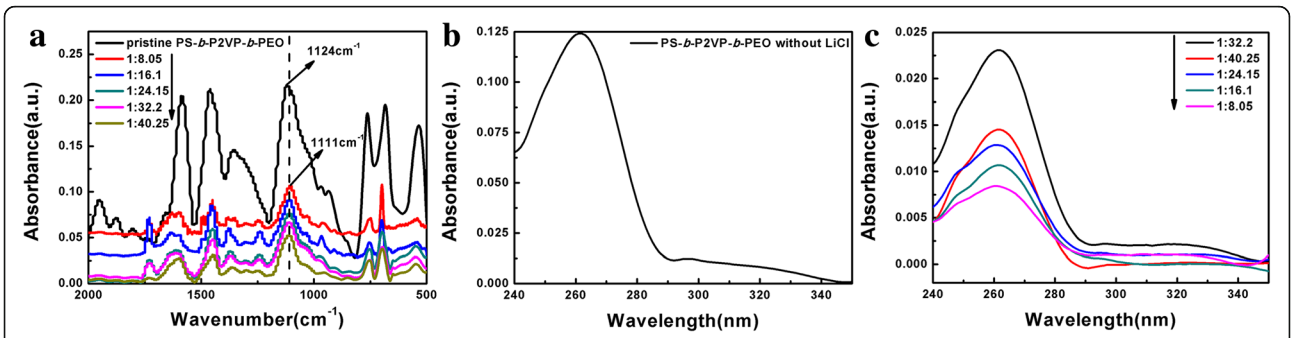

Fig. 8 (**a**) FT-IR spectra of pure PS-*b*-P2VP-*b*-PEO thin film and the thin film with LiCl-toluene; (**b**) UV-vis spectra of pure PS-*b*-P2VP-*b*-PEO thin film; (**c**) UV-vis spectra of PS-*b*-P2VP-*b*-PEO thin film with LiCl-toluene

and the PEO blocks effectively increased due to the increase of LiCl-toluene, resulting in the obvious swelling in PEO domains [32–36].

Analysis of Competitive Interactions of Li^+ ions with PEO and P2VP Blocks

It is noteworthy that the competitive interactions of Li^+ ions with both the PEO and P2VP blocks exist in PS-*b*-P2VP-*b*-PEO/LiCl hybrids [3]. The interaction between the Li^+ ions and the PEO blocks was characterized by FT-IR (Fig. 8a). The parameter of I_a/I_f, which was the ratio of the peak intensity corresponding to the associated C-O-C to the peak intensity of free C-O-C, was used to evaluate the coordination between the Li^+ ions and the PEO blocks (Table 1) [37, 38]. The C-O-C stretching vibration changed from 1124 to 1111 cm^{-1}. The value of I_a/I_f increased with the doped LiCl increasing, indicating that the loading of Li^+ ions in PEO blocks increased when the molar ratio ([Li^+]:[O + N]) decreased from 1:40.25 to 1:8.05.

The UV-vis spectra of various PS-*b*-P2VP-*b*-PEO thin films are illustrated in Fig. 8b, c. The absorption peak at 262 nm was assigned to pyridine groups and phenyl groups of PS-*b*-P2VP-*b*-PEO [39]. Based on the previous study [24], the obvious change of the intensity was attributed to the coordination between Li^+ ions and pyridine groups. The intensities of absorption peak at 262 nm with different samples were summarized in Table 2. The intensities of absorption peak at 262 nm for PS-*b*-P2VP-*b*-PEO thin films with LiCl (Fig. 8c) were weaker than the pure film (Fig. 8b). When the molar ratio ([Li^+]:[O + N]) was 1:40.25, 1:24.15, 1:16.1 and 1:8.05, the intensity of absorption peak at 262 nm decreased with the LiCl addition increasing (Fig. 8c), indicating that more and more Li^+ ions were coordinated with the P2VP blocks and PEO blocks. However, when the molar ratio ([Li^+]:[O+N]) was 1:32.2, the absorption peak at 262 nm was stronger than the molar ratio 1:40.25. The reason should be that most of Li+ ions were loaded in PEO blocks but not P2VP blocks when the molar ratio was about 1:32.2, and the least LiCl was loaded in P2VP blocks at this molar ratio ([Li^+]:[O + N] = 1:32.2) compared with other thin films with LiCl.

Table 1 The data of I_a/I_f for different PS-*b*-P2VP-*b*-PEO/LiCl hybrids in LiCl-toluene

[Li^+]:[O + N]	I_a/I_f
1:40.25	0.2522
1:32.2	0.3165
1:24.15	0.3670
1:16.1	0.4266
1:8.05	0.4908

Table 2 The intensity of absorption peak at 262 nm with different PS-*b*-P2VP-*b*-PEO thin films

Samples	Intensity at 262 nm (a.u.)
PS-*b*-P2VP-*b*-PEO thin film	0.123
1:32.2	0.023
1:40.25	0.015
1:24.15	0.013
1:16.1	0.011
1:8.05	0.009

The PS-*b*-P2VP-*b*-PEO thin films without and with LiCl-toluene ([Li^+]:[O + N] = 1:32.2) were analyzed by X-ray photoelectron spectroscopy (XPS) (Figs. 9 and 10). XPS survey spectra (Fig. 9) of PS-*b*-P2VP-*b*-PEO with LiCl confirmed the presence of C, O, N, Li and Cl. The C1s binding energy in C-C bonds was 284.78 eV. The O1s binding energy of C-O-C in PEO block was 533.08 eV, and N1 s binding energy based on the P2VP block was 399.48 eV. The Cl2p appeared at 198.28 eV, and Li1s appeared in 55.88 eV. High resolution XPS spectra of N1 s binding energy and O1s binding energy in PS-*b*-P2VP-*b*-PEO with and without LiCl were shown in Fig. 10a, b. The N1 s binding energy in PS-*b*-P2VP-*b*-PEO without LiCl was 398.88 eV, but the binding energy in the thin film with LiCl was 399.48 eV. The O1s binding energy in PS-*b*-P2VP-*b*-PEO without LiCl was 532.78 eV, but the binding energy in the thin film with LiCl was 533.08 eV. These shifts in binding energy were consequences of electron withdrawing effect caused by the coordination between Li^+ and PS-*b*-P2VP-*b*-PEO [40], validating the presence of Li element in the thin film after Li^+ ions were loaded. These results were essentially identical to the results in Fig. 8.

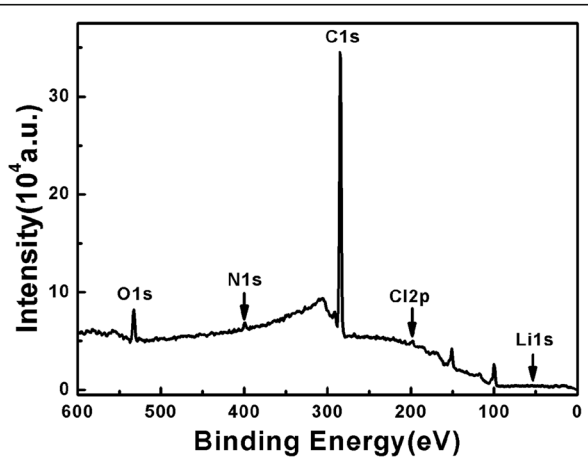

Fig. 9 XPS survey spectra of PS-*b*-P2VP-*b*-PEO thin film with LiCl-toluene

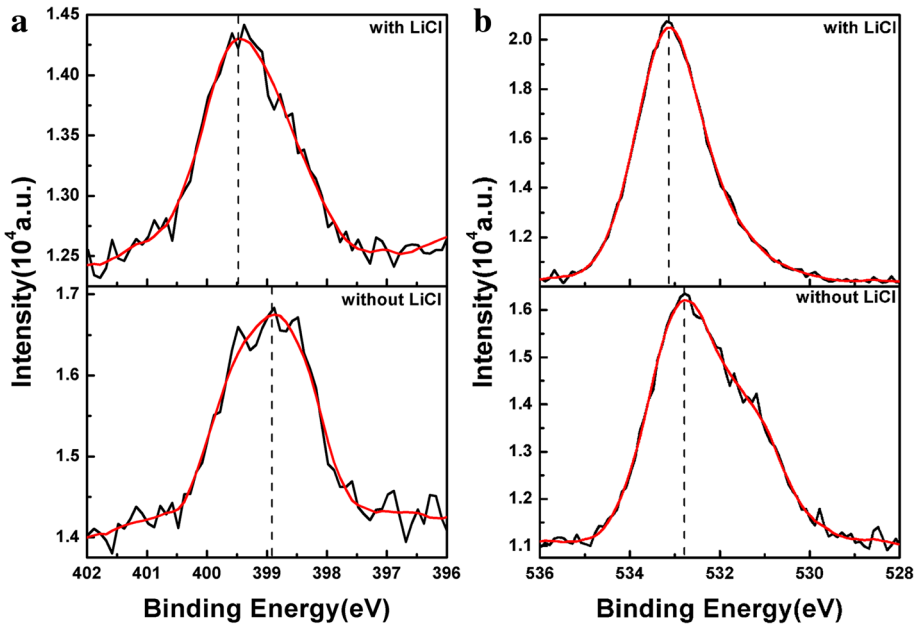

Fig. 10 High-resolution XPS spectra of (**a**) N1 s binding energy and (**b**) O1s binding energy in PS-*b*-P2VP-*b*-PEO with and without LiCl-toluene

Conclusions

In this study, we present a simple approach to fabricate ordered nanopatterns of ion/triblock copolymers hybrids without post-processing. This work demonstrated that toluene could be used as co-solvents for LiCl in short time. An order-to-disorder transition was triggered by varying the addition of LiCl-toluene with ultrasonic treatment. And ordered microphase-separated nanopatterns of cylindrical array and stripes were obtained. The mechanism of the morphological transition was due to the LiCl loaded in different ion-dissolving blocks. This rapid synthesis might boost future studies of ion/triblock copolymers hybrids because of the advantage of ultrasonic as compared to the conventional routes. Furthermore, this approach has potential applications in developing ultra-small devices via techniques such as pattern transfer owing to its simplicity, effectiveness and low cost, especially regarding to fabrication time.

Abbreviations

[Li^+]:[O + N]: the molar ratio of Li^+ ions to the total number of oxygen atoms (O) in PEO block and the nitrogen atoms (N); AFM: Atomic force microscope; CETC: China Electronics Technology Group Corporation; diBCPs: diblock copolymers; DMF: N,N-Dimethylform amide; FT-IR: Fourier transform infrared; HRTEM: High resolution transmission electron microscopy; LiCl: lithium chloride; LiOH: Lithium hydroxide; PCL: poly(ε-caprolactone); PMMA: polymethyl methacrylate; PS: polystyrene; PS-*b*-P2VP-*b*-PEO: polystyrene-*block*-poly(2-vinylpyridine)-*block*-poly(ethylene oxide); PVP: polyvinyl pyridine; triBCPs: triblock copolymers; UV-vis: Ultraviolet–visible; XPS: X-ray photoelectron spectroscopy

Acknowledgements

This work was supported by the National Natural Science Foundation of China (Grant No. 51273048 and 51203025), the Natural Science Foundation of Guangdong province (Grant No. S2012040007725) and the Pearl River S&T Nova Program of Guangzhou (201710010144).

Funding

National Natural Science Foundation of China (Grant No. 51273048 and 51,203,025).
Natural Science Foundation of Guangdong province (Grant No. S2012040007725).
Pearl River S&T Nova Program of Guangzhou (201710010144).

Authors' Contributions

HH, GY, and XZ designed the experiment and measurements. HH, BZ, MZ, and YZ executed the experiments. HH, GY, XZ, BZ, HL, WL, MZ, and YZ examined the written report. All authors read and approved the final manuscript.

Ethics Approval and Consent to Participate

Not applicable.

Consent for Publication

Not applicable.

Competing Interests

The authors declare that they have no competing interests.

Publisher's Note

Springer Nature remains neutral with regard to jurisdictional claims in published maps and institutional affiliations.

Received: 22 April 2017 Accepted: 1 August 2017
Published online: 15 August 2017

References

1. Young WS, Eppslll TH (2009) Salt doping in PEO-containing block copolymers: counterion and concentration effects. Macromolecules 42: 2672–2678
2. Ham SJ, Shin CH, Kim E, Ryu DY, Jeong U, Russell TP, Hawker CJ (2008) Microdomain orientation of PS-*b*-PMMA by controlled interfacial interactions. Macromolecules 41:6431–6437

3. Huang J, Tong ZZ, Zhou B, Xu JT, Fan ZQ (2013) Salt-induced microphase separation in poly (ε-caprolactone)-b-poly (ethylene oxide) block copolymer. Polymer 54:3098–3106
4. Diao Z, Kraus M, Brunner R, Dirks JH, Spatz JP (2016) Nanostructured stealth surfaces for visible and near-infrared light. Nano Lett 16:6610–6616
5. Rahman A, Ashraf A, Xin HL, Tong X, Sutter P, Eisaman MD, Black CT (2015) Sub-50-nm self-assembled nanotextures for enhanced broadband antireflection in silicon solar cells. Nat Commun 6:1–6
6. Ghoshal T, Ntaras C, Connell JO, Shaw MT, Holmes JD, Avgeropoulos A, Morris MA (2016) Fabrication of ultra-dense sub-10 nm in-plane Si nanowire arrays by using a novel block copolymer method: optical properties. Nano 8:2177–2187
7. Bang J, Kim SH, Drockenmuller E, Misner MJ, Russell TP, Hawker CJ (2006) Defect-free nanoporous thin films from ABC triblock copolymers. J Am Chem Soc 128:7622–7629
8. Tang CB, Bang J, Stein GE, Fredrickson GH, Hawker CJ, Kramer EJ, Sprung M, Wang J (2008) Square packing and structural arrangement of ABC triblock copolymer spheres in thin films. Macromolecules 41:4328–4339
9. Bita I, Yang JKW, Ross CA, Thomas EL, Berggren KK (2008) Graphoepitaxy of self-assembled block copolymers on two-dimensional periodic patterned templates. Science 321:939–943
10. Park S, Lee DH, Xu J, Kim B, Hong SW, Jeong U, Xu T, Russell TP (2009) Macroscopic 10-terabit-per-square-inch arrays from block copolymers with lateral order. Science 323:1030–1033
11. Xu JP, Wang K, Li JY, Zhou HM, Xie XL, Zhu JT (2015) ABC triblock copolymer particles with tunable shape and internal structure through 3D confined assembly. Macromolecules 48:2628–2636
12. Xu JP, Yang Y, Wang K, Li JY, Zhou HM, Xie XL, Zhu JT (2015) Additives induced structural transformation of ABC Triblock copolymer particles. Langmuir 31:10975–10982
13. Zhang KR, Talley SJ, Yu YP, Moore RB, Murayama M, Long TE (2016) Influence of nucleobase stoichiometry on the self-assembly of ABC triblock copolymers. Chem Commun 52:7564–7567
14. Matsushita Y (2007) Creation of hierarchically ordered nanophase structures in block polymers having various competing interactions. Macromolecules 40:771–776
15. Xue T, Xu CL, Zhao DD, Li XH, Li HL (2007) Electro deposition of mesoporous manganese dioxide supercapacitor electrodes through self-assembled triblock copolymer templates. J Power Sources 164:953–958
16. Qiao YL, Ferebee R, Lee B, Mitra I, Lynd NA, Hayat J, Stein GE, Bockstaller MR, Tang CB (2014) Symmetric poly (ethylene oxide-b-styrene-b-isoprene) triblock copolymers: synthesis, characterization, and self-assembly in bulk and thin film. Macromolecules 47:6373–6381
17. Kim SH, Misner MJ, Yang L, Gang O, Ocko BM, Russell TP (2006) Salt complexation in block copolymer thin films. Macromolecules 39:8473–8479
18. Ghoshal T, Maity T, Godsell JF, Roy S, Morris MA (2012) Large scale monodisperse hexagonal arrays of superparamagnetic iron oxides nanodots: a facile block copolymer inclusion method. Adv Mater 24:2390–2397
19. Ghoshal T, Senthamaraikannan R, Shaw MT, Holmes JD, Morris MA (2012) "in situ" hard mask materials: a new methodology for creation of vertical silicon nanopillar and nanowire arrays. Nano 4:7743–7750
20. Wang JY, Chen W, Roy C, Sievert JD, Russell TP (2008) Influence of ionic complexes on phase behavior of polystyrene-b-poly (methyl methacrylate) copolymers. Macromolecules 41:963–969
21. Yang JX, He WN, Xu JT, Du BY, Fan ZQ (2014) Influence of different inorganic salts on crystallization-driven morphological transformation of PCL-*b*-PEO micelles in aqueous solutions. Chinese J Polym Sci 32:1128–1138
22. He J, Wang JY, Xu J, Tangirala R, Shin D, Russell TP, Li X, Wang J (2007) On the influence of ion incorporation in thin films of block copolymers. Adv Mater 19:4370–4374
23. Lee DH, Kim HY, Kim JK (2006) Swelling and shrinkage of lamellar domain of conformationally restricted block copolymers by metal chloride. Macromolecules 39:2027–2030
24. Sadoway DR, Huang B, Trapa PE, Soo PP, Bannerjee P, Mayes AM (2001) Self-doped block copolymer electrolytes for solid-state, rechargeable lithium batteries. J Power Sources 97:621–623
25. Nakamura I, Wang ZG (2012) Salt-doped block copolymers: ion distribution, domain spacing and effective χ parameter. Soft Matter 8:9356–9367
26. Ren CL, Nakamura I, Wang ZG (2015) Effects of ion-induced cross-linking on the phase behavior in salt-doped polymer blends. Macromolecules 49:425–431
27. Wang JY, Chen W, Russell TP (2008) Ion-complexation-induced changes in the interaction parameter and the chain conformation of PS-*b*-PMMA copolymers. Macromolecules 41:4904–4907
28. Wang JY, Chen W, Sievert JD, Russell TP (2008) Lamellae orientation in block copolymer films with ionic complexes. Langmuir 24:3545–3550
29. Zhao JP, Pispas S, Zhang GZ (2009) Effect of sonication on polymeric aggregates formed by poly(ethylene oxide)-based amphiphilic block copolymers. Macromol Chem Phys 210:1026–1032
30. Williges C, Chen WW, Morhard C, Spatz JP, Brunner R (2013) Increasing the order parameter of quasi-hexagonal micellar nanostructures by ultrasound annealing. Langmuir 29:989–993
31. Ethirajan A, Punniyakoti S, Olieslaeger MD, Wagner P, Boyen HG (2013) Ultrafast self-assembly using ultrasound: a facile route to the rapid fabrication of well-ordered dense arrays of inorganic nanostructures. Angew Chem Int Edit 52:9709–9713
32. Ghoshal T, Ntaras C, Shaw MT, Holmes JD, Avgeropoulos A, Morris MA (2015) A vertical lamellae arrangement of sub-16 nm pitch (domain spacing) in a microphase separated PS-*b*-PEO thin film by salt addition. J Mater Chem C 3:7216–7227
33. Rosedale JH, Bates FS, Almdal K, Mortensen K, Wignall GD (1995) Order and disorder in symmetric diblock copolymer melts. Macromolecules 28:1429–1443
34. Almdal K, Mortensen K, Ryan AJ, Bates FS (1996) Order, disorder, and composition fluctuation effects in low molar mass hydrocarbon-poly(dimethylsiloxane) diblock copolymers. Macromolecules 29:5940–5947
35. Gunkel I, Thurn-Albrecht T (2011) Thermodynamic and structural changes in ion-containing symmetric diblock copolymers: a small-angle X-ray scattering study. Macromolecules 45:283–291
36. Noro A, Sageshima Y, Arai S, Matsushita Y (2010) Preparation and morphology control of block copolymer/metal salt hybrids via solvent-casting by using a solvent with coordination ability. Macromolecules 43:5358–5364
37. Huang J, Wang RY, Tong ZZ, Xu JT, Fan ZQ (2014) Influence of ionic species on the microphase separation behavior of PCL-b-PEO/salt hybrids. Macromolecules 47:8359–8367
38. Huang J, Tong ZZ, Zhou B, Xu JT, Fan ZQ (2014) Phase behavior of $LiClO_4$-doped poly (ε-caprolactone)-b-poly(ethylene oxide) hybrids in the presence of competitive interactions. Polymer 55:1070–1077
39. Shin WJ, Kim JY, Cho G, Lee JS (2009) Highly selective incorporation of SiO_2 nanoparticles in PS-*b*-P2VP block copolymers by quaternization. J Mater Chem 19:7322–7325
40. Oded M, Kelly ST, Gilles MK, AHE M¨l, Shenhar R (2016) Periodic nanoscale patterning of polyelectrolytes over square centimeter areas using block copolymer templates. Soft Matter 12:4595–4602

Submit your manuscript to a SpringerOpen journal and benefit from:

- ► Convenient online submission
- ► Rigorous peer review
- ► Open access: articles freely available online
- ► High visibility within the field
- ► Retaining the copyright to your article

Submit your next manuscript at ► springeropen.com